Clim Dyn (2009) 33:461–475
DOI 10.1007/s00382-008-0503-6

A model study of the Little Ice Age and beyond: changes in ocean heat content, hydrography and circulation since 1500

Jan Sedláček · Lawrence A. Mysak

Received: 7 March 2008 / Accepted: 26 November 2008 / Published online: 19 December 2008

Abstract The Earth System Climate Model from the University of Victoria is used to investigate changes in ocean properties such as heat content, temperature, salinity, density and circulation during 1500 to 2000, the time period which includes the Little Ice Age (LIA) (1500–1850) and the industrial era (1850–2000). We force the model with two different wind-stress fields which take into account the North Atlantic Oscillation. Furthermore, temporally varying radiative forcings due to volcanic activity, insolation changes and greenhouse gas changes are also implemented. We find that changes in the upper ocean (0–300 m) heat content are mainly driven by changes in radiative forcing, except in the polar regions where the varying wind-stress induces changes in ocean heat content. In the full ocean (0–3,000 m) the wind-driven effects tend to reduce, prior to 1700, the downward trend in the ocean heat content caused by the radiative forcing. Afterwards no dynamical effect is visible. The colder ocean temperatures in the top 600 m during the LIA are caused by changes in radiative forcing, while the cooling at the bottom is wind-driven. The changes in salinity are small except in the Arctic Ocean. The reduced salinity content in the subsurface Arctic Ocean during the LIA is a result from reduced wind-driven inflow of saline water from the North Atlantic. At the surface of the Arctic Ocean the changes in salinity are caused by changes in sea–ice thickness. The changes in density are a composite picture of the temperature and salinity changes. Furthermore, changes in the meridional overturning circulation (MOC) are caused mainly by a varying wind-stress forcing; the additional buoyancy driven changes due to the radiative forcings are small. The simulated MOC is reduced during the LIA as compared to the industrial era. On the other hand, the ventilation rate in the Southern Ocean is increased during the LIA.

Keywords Hydrography · Ocean circulation · Little Ice Age · Radiative forcing · Wind-stress forcing

J. Sedláček · L. A. Mysak
Earth System Modelling Group, Department of Atmospheric and Oceanic Sciences, McGill University, Montreal, QC H3A 2K6, Canada

Present Address:
J. Sedláček (✉)
Institute for Atmospheric and Climate Science, Swiss Federal Institute of Technology Zurich, Universitätstrasse 16, 8092 Zurich, Switzerland
e-mail: jan.sedlacek@env.ethz.ch

1 Introduction

The 'Little Ice Age' (LIA), which occurred roughly from 1500 to 1850, was the latest and most dramatic cold event in a sequence of multi-centennial cold periods over the last 4 kyr (Grove 2004). The LIA was followed by a warming trend during the industrial era. Although regional differences exist in the timing of the cold episodes (Bradley and Jones 1995) and the sign of the (reconstructed) temperature anomalies in different locations may differ seasonally (Pfister 1995), the hemispheric and global mean annual air temperatures show a cooling during the LIA. The ocean did not play a dominant role in creating the negative air temperature anomalies during the LIA (Jones and Mann 2004). However, the colder air temperatures at the atmosphere–ocean boundary may have had an impact on such ocean conditions as the sea–ice cover, heat content, hydrography and circulation. Indeed, according to the model study of Sedláček and Mysak (2008) (henceforth SM2008), these colder temperatures certainly resulted in a more extensive

and thicker Arctic sea–ice cover during the LIA. In this paper, the work of SM2008 is extended to investigate the impact of the LIA on the ocean heat content, hydrography and meridional overturning circulation (MOC).

From an analysis of phosphate and chlorofluorocarbon tracers, Broecker et al. (1999) and Broecker (2000) hypothesized that the formation of Antarctic Bottom Water (AABW) was enhanced during the LIA. They suggested that during the LIA, both high-latitude ocean regions ventilated roughly at the same rate. By way of contrast, in the Southern Ocean today, the ventilation rate is much smaller than in the northern oceans.

According to foraminifera data, the Florida Current transport was estimated to be 10% smaller during the LIA as compared to the transport today (Lund et al. 2006). Changes in both the wind-driven circulation and the AMOC (Atlantic meridional overturning circulation) contributed to this reduction; however, the relative magnitudes of the reductions associated with each circulation cannot be determined. According to sedimentological and paleochemical data, Keigwin and Boyle (2000) reported that nutrient-rich circumpolar waters replaced the North Atlantic Deep Water (NADW) during the LIA in the deep North Atlantic.

During the LIA the sea surface temperature was estimated to be about 1°C colder than today in the Sargasso Sea (Keigwin 1996). Proxy measurements indicate a more saline tropical Pacific sea surface (Hendy et al. 2002) and reduced salinity in Indio-Pacific region (Newton et al. 2006) during the late LIA as compared to the twentieth century, mainly due to advection and wind-induced evaporation changes.

Crowley et al. (2003) used a simple upwelling-diffusion ocean model coupled to an energy balance model for the atmosphere to determine the ocean heat content changes from 1000 to 2000 in response to radiative forcing changes (in volcanic activity, insolation, tropospheric aerosol loading and greenhouse gases). Their simulation showed that the heat content of the full ocean (0–3,000 m) increased by 5×10^{23} J from the LIA to the end of the twentieth century, and they estimated that this would imply a 7-cm sea level rise after 1840. To the best of our knowledge, there is no other published model study of the ocean conditions during the LIA and their changes afterward.

In this paper, we extend the work of Crowley et al. (2003) by using the Earth System Climate Model from the University of Victoria (UVic ESCM) (Weaver et al. 2001) to examine the role of ocean dynamics in producing ocean heat content and hydrographic changes during the LIA and beyond. More specifically, we assess mechanisms which could have led to the above-mentioned observed changes in the ocean and investigate the impact of the colder LIA surface air temperatures on such ocean properties as temperature, salinity, density and circulation. Also, we assess the validity of the Broecker et al. (1999) and Broecker (2000) hypothesis of an increased southern ventilation rate during the LIA.

Stommel (1961) showed with a simple box model and Marotzke et al. (1988) with a meridional plane model, that a north-south gradient in temperature or salinity and hence density can produce an AMOC. However, the wind stress over the Atlantic Ocean is also an important driver for the AMOC (Timmermann and Goosse 2004). The wind forcing maintains the horizontal density gradients by transporting salt and heat. Toggweiler and Samuels (1995) and Rahmstorf and England (1997) showed that the wind forcing in the Southern Ocean is capable of influencing the NADW formation. While Toggweiler and Samuels (1995) argue that there is a linear relationship between the NADW outflow from the Atlantic basin and the Ekman drift in the Southern Hemisphere, Rahmstorf and England (1997) showed that this is the case only in a model with restoring boundary conditions. The inclusion of thermal feedbacks changes the relationship between the NADW outflow and the Southern Ocean winds. Hence, the wind over the Southern Ocean modifies the NADW formation instead of driving the AMOC. Unfortunately, it is not possible to determine what part of the global ocean circulation is due to wind forcing and what part is due to buoyancy effects (Gill 1982).

To determine the role of winds in forcing long-term changes in the ocean properties, we use two different wind-stress forcings from SM2008 which take into account the North Atlantic Oscillation (NAO). This allows us to determine the robustness of the long-term changes due to atmospheric dynamic influences. Additionally, we use radiative forcings from Crowley (2000). This allows us to identify which changes are due to variations in the wind-stress forcing and which are due to variations in the radiative forcings.

The remainder of the paper is structured as follows. In Sect. 2 we present the model, the wind-stress fields and the experimental setup. In Sect. 3 the results of the simulations are presented. Then, in Sect. 4 we discuss the shortcomings of our simulations and present possible mechanisms which could explain the Broecker et al. (1999) and Broecker (2000) hypothesis. We summarize our findings in Sect. 5.

2 Description of the model and the forcing fields

2.1 The UVic ESCM

The first release of the UVic ESCM is described in Weaver et al. (2001). In this study we use the version 2.6, which

consists of oceanic, atmospheric and sea–ice components. The resolution of the model is 3.6° zonally and 1.8° meridionally. The UVic ESCM does not use explicit flux adjustments and the freshwater and total energy drifts are close to machine precision (Weaver et al. 2001).

The ocean model is the 3-D primitive-equation general circulation model (GCM) MOM 2.2 (Pacanowski 1995) with 19 unequally spaced layers in the vertical. The near-surface layer is 50 m thick and the bottom layer is 518 m thick. In this study we use a modified Bryan and Lewis (1979) vertical diffusivity distribution. The diffusivity k_v in the thermocline is 6×10^{-5} m^2 s^{-1} and in the deep ocean $k_v = 1.6 \times 10^{-4}$ m^2 s^{-1}. The atmospheric model is an energy-moisture balance model (EMBM) (Fanning and Weaver 1996) with heat and moisture transport parameterized by a diffusion term. In this model, climatological winds are used for moisture advection and the calculation of the turbulent fluxes. The sea–ice component is a dynamic-thermodynamic model. The thermodynamic part uses the zero-layer Semtner model (Bitz et al. 2001), and the sea–ice dynamic part uses the granular sea–ice model GRAN (Sedláček et al. 2007). The GRAN is founded on the physics of a slowly deforming granular material. The yield curve is based on a Mohr–Coulomb failure criterion, and a non-normal flow rule is used (Tremblay and Mysak 1997). Although the UVic ESCM provides a parameterization for brine convection, this option is not used in this study. However, salt is rejected during sea–ice formation.

In the UVic ESCM, the runoff flows instantaneously through 32 river basins into the ocean. Furthermore, Iceland is removed from the ocean domain to improve the North Atlantic Drift heat transport. Also, Bering Strait is closed due to the coarse resolution. The closing of Bering Strait reduces the freshwater flux into the North Atlantic and increases the strength of the AMOC (A. Jahn, personal communication, 2008). The climatological sea–ice area extends too far south (e.g., Weaver et al. 2001; Mysak et al. 2005; Sedláček et al. 2007). However, the observed thickness distribution in the Arctic Ocean is captured quite well (e.g., Mysak et al. 2005; Sedláček et al. 2007). Although the NADW formation region is located too far south in the UVic ESCM, it is still sensitive to short-term sea–ice export variations from the Arctic (e.g., Holland et al. 2001; Mysak et al. 2005).

Because the atmospheric component of the model is an EMBM, the wind-stress forcing must be prescribed, as well as the atmospheric CO_2 concentration.

2.2 Forcing fields

Here we give only a brief description of how the wind-stress forcings [the Analog Winter approach (ANAW) and the Decomposition approach (DECOMP)] that we use in this paper are obtained. For a more thorough description of the construction and differences of the wind-stress fields, we refer the reader to SM2008, where two additional wind-stress fields are produced and used with the UVic ESCM. However, in this paper only the two wind-stress fields described below are used. Below we also briefly describe the radiative forcings used in this study.

2.2.1 *Analog winter approach (ANAW)*

Luterbacher et al. (2002a) derived the NAO index back to 1500 from reconstructed sea-level pressures derived by Luterbacher et al. (2002b). The reconstructed NAO index is calculated as the difference of the sea-level pressure averaged over a 5° × 5° longitude-latitude box over the Azores from that over Iceland. The index for the period from 1500 to 1659 has a seasonal resolution, whereas after 1659, the resolution is monthly. From Luterbacher et al.'s NAO index reconstruction, we calculate the winter NAO index (December through March). Furthermore, during the period 1950 to 1999, the wind-stress fields are known from the National Centers for Environmental Prediction/National Center for Atmospheric Research (NCEP/NCAR) re-analysis along with the winter NAO index values. To build a continuous wind-stress field over the earlier centuries, we pick a certain year during this time and determine its corresponding winter NAO index value. For instance, the year 1605 has a winter NAO index value of 0.55. Next, we search for the year with the closest winter NAO index value in the period between 1950 and 1999. In this case it would be 1972, which has a winter NAO index value of 0.56. We then copy the monthly mean wind stresses from 1972 to 1605.

In Fig. 1a the mean wind-stress curl of the ANAW run is plotted for the LIA, and in Fig. 1c the changes of the wind-stress curl between the LIA and industrial era are shown. The changes show that the wind-stress curl was stronger almost everywhere on the globe during the LIA as compared to the industrial era.

2.2.2 *Decomposition approach (DECOMP)*

First, the annual climatology (τ_0) is computed using the NCEP/NCAR re-analysis wind-stress data (τ) for the period 1950 to 1999. Over the same period at each grid point the seasonal and monthly anomalies of the zonal and meridional directions are computed using τ_0 and τ. These anomalies are then regressed against the seasonal and monthly NAO from 1950 to 1999 to get τ_{NAO}. The τ_{NAO} field shows a large signal due to the NAO around the North Atlantic region. In the other areas of the globe, the NAO signal in τ_{NAO} is weak. Finally, a remaining wind-stress field (τ_{rem}) is computed as follows: $\tau_{\mathrm{rem}} = \tau - (\tau_0 + \mathrm{NAOI} \times \tau_{\mathrm{NAO}})$, where NAOI is the NAO index from 1950 to 1999.

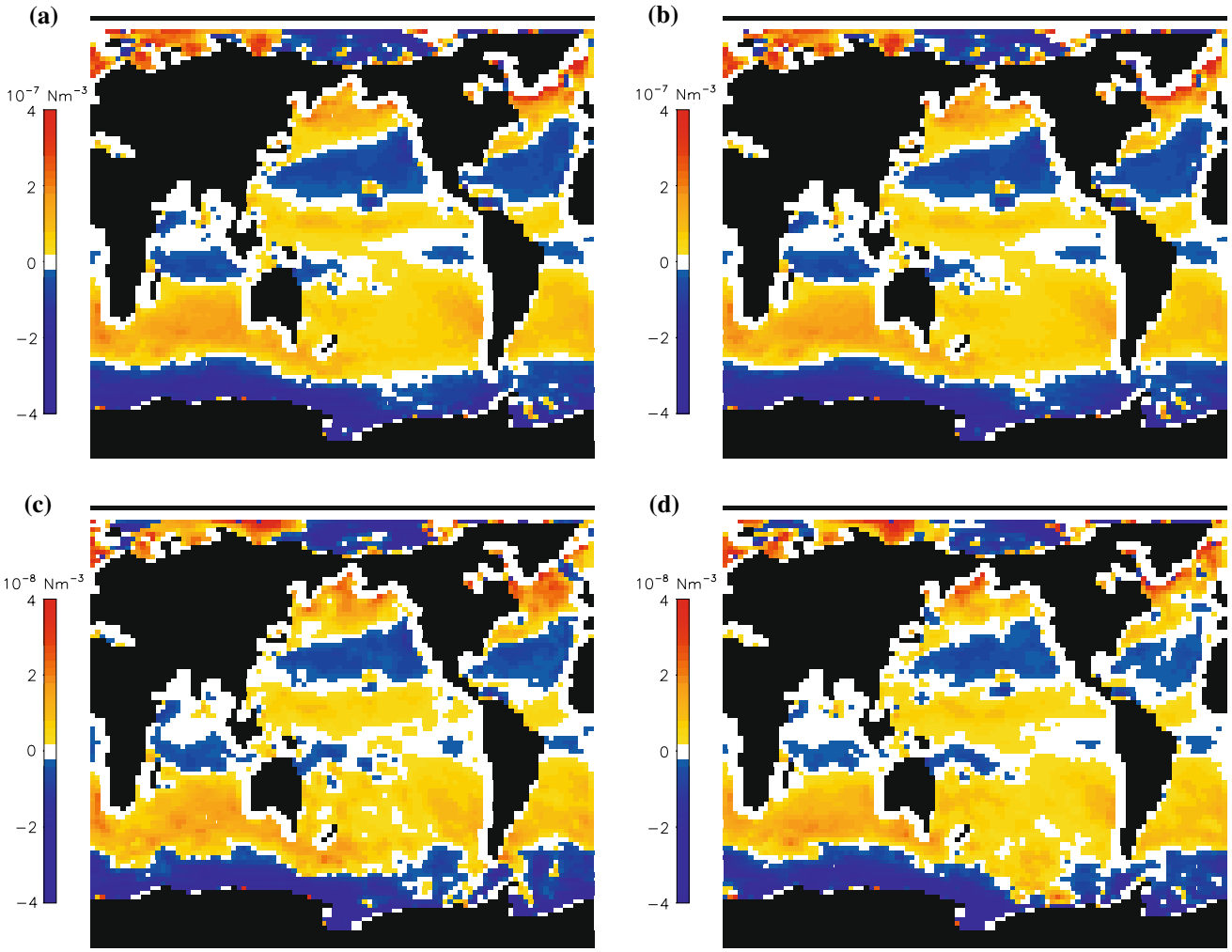

Fig. 1 The mean wind-stress curl during the LIA computed from the ANAW wind-stress field (**a**), and from the DECOMP wind-stress field (**b**). The mean of the wind-stress curl using the ANAW wind-stress field for 1500–1850 minus the mean of the same for 1850–2000 (**c**), and the same difference but with the DECOMP wind-stress field, (**d**). Note that the values in **c** and **d** are an order of magnitude smaller than in **a** and **b**

To construct the DECOMP wind field for the 500-year period, we take $\tau_{\mathrm{DECOMP}} = \tau_0 + \mathrm{NAOI} \times \tau_{\mathrm{NAO}} + \tau^*_{\mathrm{rem}}$, where NAOI in this case is changing with the temporal resolution of Luterbacher et al.'s NAO index reconstruction and τ^*_{rem} is a random permutation of the τ_{rem}'s from the period 1950 to 1999. This is equivalent to prescribing a 'random noise' where the main wind-stress direction is preserved. The term τ_{rem} is quite large and dominates the DECOMP wind-stress field.

Figure 1b and d show the DECOMP wind-stress curl of the LIA and the difference between the LIA and the industrial period. The mean wind-stress curl pattern of the LIA from the DECOMP run (Fig. 1b) is very similar to the pattern of the ANAW run (Fig. 1a). As in the ANAW case, the wind-stress curl was stronger during the LIA everywhere on the globe with the exception of the Southern Pacific, near the Amundsen Sea, where the wind-stress was decreased during the LIA as compared to the industrial era (Fig. 1d).

2.2.3 *Radiative forcings*

Crowley (2000) used four external radiative forcings in a simple climate model to simulate changes in the Northern Hemisphere temperature during the last millennium. In this study, only three of these external forcings are used: volcanic activity, insolation changes and greenhouse gas changes. The fourth forcing, namely, the radiative cooling due to tropospheric aerosols in the twentieth century, is neglected. For further details on the reconstructions of the radiative forcings, we refer the reader to Crowley (2000) and the references therein. The time series of the radiative forcings used are shown in Fig. 1 of SM2008. We note that the version of the UVic ESCM used for this study does not

include vegetation and thus forcings due to land cover changes and deforestation are neglected.

2.2.4 Experimental setup

The spin-up phase is started 200 years prior to the actual run (i.e., at year 1300) from an equilibrium run provided with the UVic ESCM. The equilibrium run was done with climatological NCEP/NCAR re-analysis wind-stress fields and a CO_2 concentration of 280 ppm. During the spin-up, the monthly mean wind-stress fields are specified from a random permutation of the years 1950 to 1999 of the NCEP/NCAR re-analysis. This is done in order to reduce any biases due to different modes in the atmospheric circulation. Futhermore, the insolation is set constant and the volcanic activity is zero during the spin-up. A comparison with a longer spin-up which was performed later during the investigation suggests that a 200-year spin-up is sufficient for this study (not shown).

We performed two simulations for each wind-stress field: (1) a control run (CONTR) with constant solar activity and pre-industrial greenhouse gas concentration and no volcanic activity, and (2) a radiatively forced run (VOLSOLGHG) with changing greenhouse gas concentration and solar activity, and also volcanic activity. The radiative forcings in the VOLSOLGHG runs are implemented as changes of the solar constant at the top of the atmosphere. Note that all the runs start from the same spin-up.

3 Results

SM2008 showed that with the two wind-stress reconstructions used in this study as forcing, the Northern Hemisphere surface air temperature anomalies agree well with several temperature anomaly reconstructions between 1500 and the late twentieth century (see their Fig. 3). However, there is a more pronounced simulated Northern Hemisphere cooling during the early 1800s and a larger warming after 1950 as compared to the reconstructions. A similar behavior was observed by Zorita et al. (2004) using the same radiative forcings with a fully coupled atmosphere–ocean GCM.

As stated in the introduction, the wind-driven and the buoyancy-driven circulations cannot be separated into component parts. Here, we use the term 'radiatively-driven' for changes seen in the difference between a VOLSOLGHG run and a CONTR run, and the term 'wind-driven' for changes of a CONTR run only. Note that both definitions include buoyancy-driven changes. Unless otherwise stated, the LIA is defined as the period between 1500 and 1850 and the industrial era is the period between 1850 and 2000. We will only show the results from the ANAW simulations since the results for the DECOMP simulations are similar. However, we will point out differences between the results for the two wind-stress fields when they give further insight into the behavior of the model simulations.

3.1 Ocean heat content

The heat uptake and release by the oceans is an important mechanism in long-term climate changes. The heat exchange at the ocean surface acts as a lower boundary condition for the atmosphere. Furthermore, the ocean acts as a buffer during cold or warm events.

Figure 2a shows that the changes in the upper ocean (0–300 m) heat content are driven mainly by radiative changes; the influence of changes in the wind-driven circulation on the heat content is small. (Note that all the anomalies are scaled with respect to the period 1960–1990.) Figure 2a also shows that regardless of the wind-stress forcing, the evolution of the heat content anomaly with time follows the same general shape. This

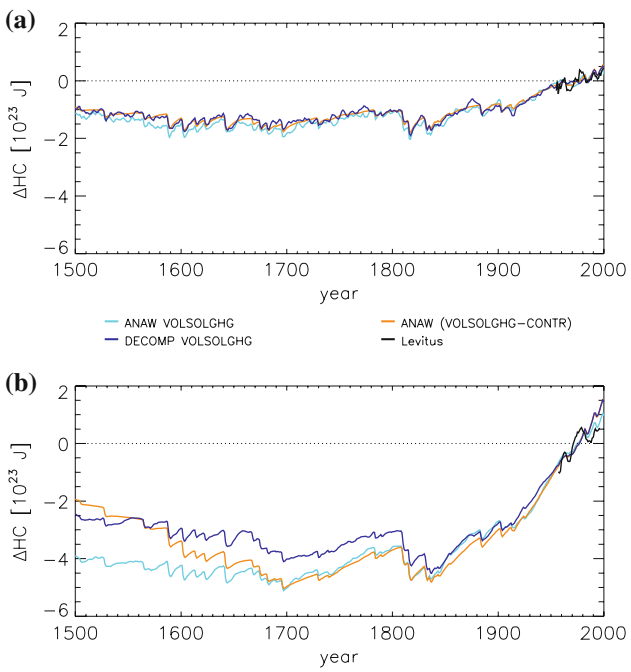

Fig. 2 Total ocean heat content anomalies (ΔHC) scaled with respect to the period 1960 to 1990 for **a** the upper ocean (0–300 m), and **b**, the full ocean (0–3,000 m). The *dark blue line* denotes the ANAW VOLSOLGHG run, the *light blue line* is the DECOMP VOLSOLGHG run, and the orange line represents the VOLSOLGHG run minus the CONTR run with the ANAW wind-stress fields. The curve for the VOLSOLGHG run minus the CONTR run with the DECOMP wind stresses is nearly identical to the *orange curve* in both panels and is thus not plotted. The *black line* represents the estimates of Levitus et al. (2005) for the period between 1955 and 2000 in **a**, and between 1957 and 1996 in **b**

suggests that the long-term changes in wind-stress forcing does not influence the global upper ocean heat content. The simulated increase in heat content after the cooling in the early 1800s corresponds to a warming of the upper ocean of about 0.7°C. The simulations follow the trend of the Levitus et al. (2005) estimates for 1955–2000 (black line in Fig. 2a) and capture well the peak starting in 1980. However, the simulated variations from 1955 to 1980 are underestimated.

The simulated heat content changes in the full ocean (0–3,000 m), on the other hand, are influenced by the wind stress (Fig. 2b). The VOLSOLGHG runs minus the CONTR runs show a downward trend in ocean heat content until 1700, a small increase until 1800, a drop in the early 1800s and then an increasing trend in the industrial era (see orange line in Fig. 2b). The downward trend until 1700 is larger than that simulated by Crowley et al. (2003). In contrast, the VOLSOLGHG runs of the ANAW and DECOMP wind-stress fields have smaller trends in the beginning of the simulation (see the light and dark blue lines in Fig. 2b). Note that the simulations started from identical initial conditions and start to diverge thereafter. However, because the curves are scaled to the mean of the period from 1960 to 1990 it appears that the runs started from different initial conditions. The anomalies between the early 1800s and the end of the twentieth century range from -5×10^{23} to 1×10^{23} J. This result is consistent with that of Crowley et al. (2003), who obtained a total range of about 5×10^{23} J with an upwelling-diffusion ocean model. Compared to the full ocean estimates of Levitus et al. (2005) for the period 1957 to 1996 (black line in Fig. 2b), the general upward trend in the last two decades is slightly overestimated.

A Hovmöller diagram of the simulated upper ocean heat content anomalies gives some insights into the nature of their spatial and temporal changes (Fig. 3). Between 50°N and 65°S the ocean heat content anomalies of the CONTR run are negative at the beginning of the simulation period and become more positive with time until 1900 (Fig. 3a). After 1900 there are again extended latitudinal ranges with notable negative anomalies. The VOLSOLGHG run (Fig. 3b) however, shows a different picture. Between 50°N and 65°S, the influence of the external radiative forcing is visible. The cooling due to large volcanos interrupt the warm patches; this can be readily seen in the early 1800s. After 1850 the upper ocean starts to warm up and is much warmer than the mean by 1930. Between 65°S and 45°S, both the CONTR and the VOLSOLGHG runs show negative heat content anomalies from 1500 to 1650 and positive heat content anomalies from 1850 to 1970. Since these anomalies patterns occur in both simulations, they are partly wind-driven. However, their magnitude is different. In the ANAW VOLSOLGHG run, panel b), the increase in heat content anomalies at these very southern latitudes from the early 1800s to the mid 1900s is 1×10^{23} J. In the ANAW CONTR run, panel a), the increase in heat content anomalies in these latitudes is roughly an order of magnitude smaller, i.e., about 4×10^{22} J.

In both polar regions, there are propagating episodic (multi-decadal) warming events throughout the simulated

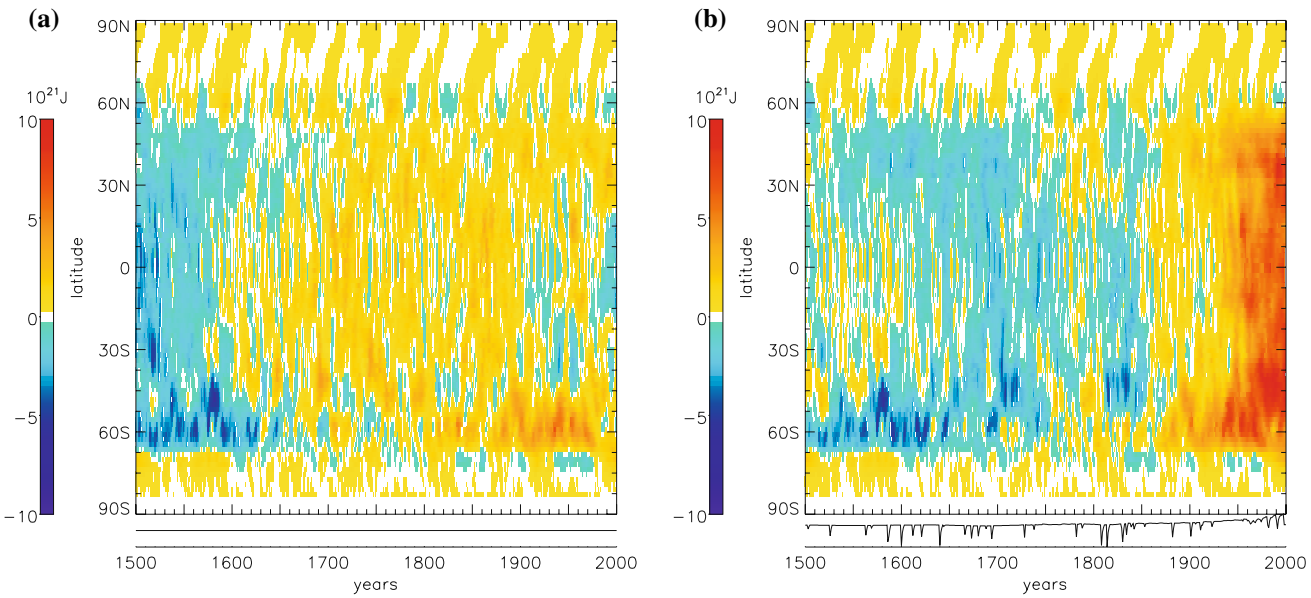

Fig. 3 Hovmöller diagram of the anomalies of the ocean heat content in the upper 300 m. The mean at each latitude is computed from 1500 to 2000. **a** ANAW CONTR run; **b**, ANAW VOLSOLGHG run. In **b** the sum of the radiative forcings is plotted at the *bottom*

period; these seem to be independent of the longer-term changes in the heat content of the rest of the ocean. A comparison of Fig. 3a and b shows that the warm events in vthe polar regions occur at approximately the same time in each simulation. Thus they are not driven by changes in radiative forcing. The DECOMP run shows similar features, however, the periodicity is different as that found in the ANAW run (not shown). It is possible that these simulated warming events are caused by advection of upper-ocean temperature anomalies created by multi-decadal variations in the wind-stress forcing field that produce changes in high-latitude ocean circulation. However, it may also be true that the warming events are reflective of an internal mode of ocean variability. It is interesting to note that oscillations in the North Atlantic on time scales of 50–85 year have been observed (e.g., Kushnir 1994; Schlesinger and Ramankutty 1994; Delworth and Mann 2000) and simulated with ocean GCMs and coupled atmosphere–ocean GCMs (e.g., Delworth et al. 1993; Delworth and Greatbatch 2000; te Raa and Dijkstra 2002; te Raa et al. 2004). Delworth et al. (1993) note that the sea surface anomalies are not confined to the North Atlantic region. They can extend well into the Arctic Ocean and even be enhanced through polar amplification effects. Delworth et al. (1993) link these oscillations to natural internal oscillations that are simulated in the MOC, and they can even be seen in an ocean model that is forced with stochastic atmospheric fluxes (Delworth and Greatbatch 2000).

In the Southern Hemisphere high-latitude warming events are simulated in the ANAW CONTR and VOLSOLGHG runs that are similar to the northern high-latitudes (Fig. 3). The DECOMP wind-stress fields produce similar warming events (not shown). These events are likely connected to the Antarctic Circumpolar Current which impedes north-south transport of ocean water. However, the origin and the mechanisms of these events needs to be further investigated.

3.2 Ocean temperature

According to our simulations, the ocean surface is on average colder during the LIA than during the industrial era (not shown). In the ice free regions, the ocean surface temperature is about 0.4°C colder over large areas as compared to the mean of the industrial era (not shown). More dramatically, in the North Atlantic, where the ice retreats in the industrial period, the ocean surface temperature increase is greater than 1°C.

During the LIA, the simulated cooling at the ocean sea surface penetrates on average to a depth of 600 m in the tropical and subtropical regions as compared to the industrial era (Fig. 4a). In the ice-free mid- to high-latitudes the cooling even penetrates to the bottom.

Figure 4b shows that the LIA cooling in the tropical and subtropical regions is mostly due to the changes in the radiative forcing. This radiatively induced cooling occurs in all three ocean basins. Below the ice-covered regions, only small changes in temperature are visible.

In the mid- to high-latitudes, wind-driven cooling occurs during the LIA, which penetrates to the bottom of the

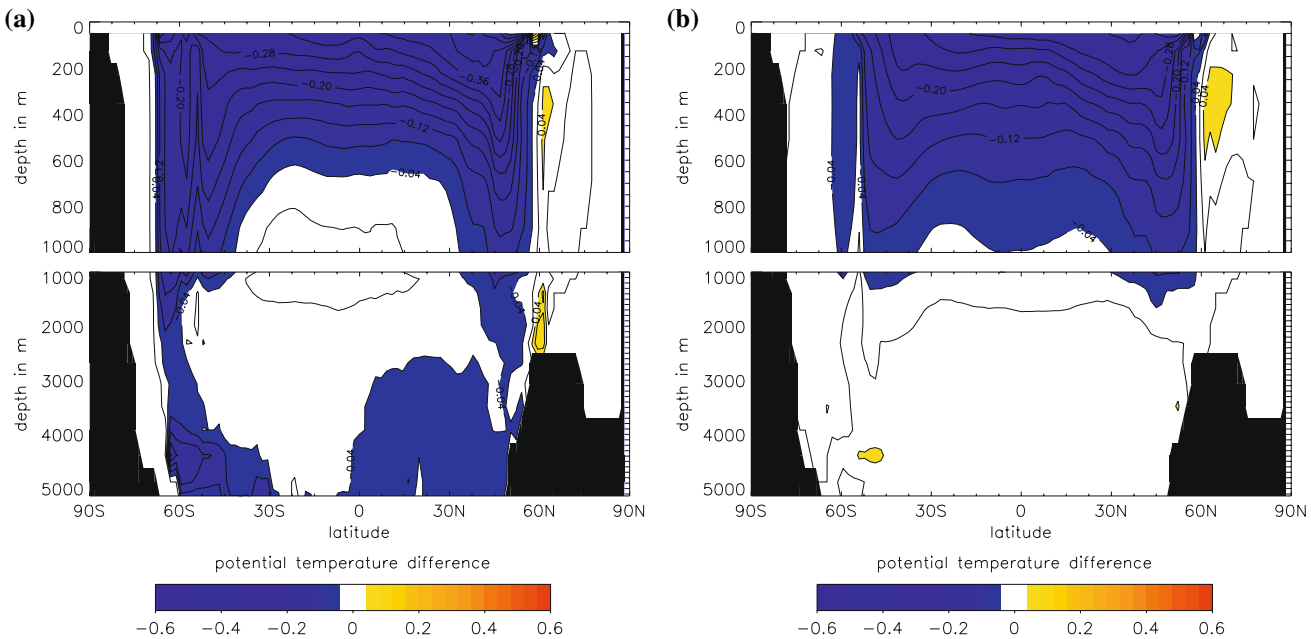

Fig. 4 Latitude-depth structure of the difference of the zonal mean annual global ocean temperature consisting of the mean of 1500 to 1850 minus the mean of 1850 to 2000 for the ANAW wind-stress field. **a** the VOLSOLGHG run; **b** the VOLSOLGHG run minus the CONTR run

ocean (Fig. 4a). Note that by definition, 'wind-driven changes' mean changes in the CONTR run (or no change in the VOLSOLGHG minus the CONTR run). This definition does not exclude buoyancy-driven changes. In the Pacific sector the southern limb carries colder water to depth and fills the bottom of the Pacific Ocean below 2,000 m during the LIA (not shown). In the Atlantic sector the colder northern limb penetrates to a depth of 2,500 m. However, in the Atlantic basin below 3,000 m there is a warm patch between 30°S and the equator during the LIA due to a warm water influx from the south (not shown). In the tropical regions at a depth of around 1,000 m, there is a layer with a small temperature increase during the LIA. The DECOMP run shows a slightly larger warming during the LIA in this region. This layer is mainly wind-driven and is most pronounced in the Indian and Pacific basins.

Sea surface temperature reconstructions from the Indio-Pacific basin show cooler temperatures during the LIA as compared to the industrial era (Newton et al. 2006). In the Tropical Pacific region, on the other hand, the temperature does not change substantially between the two periods (Hendy et al. 2002). The simulations are in agreement with the reconstructions of Hendy et al. (2002), but the temperature changes in the Indio-Pacific Basin are underestimated (not shown). However, the cool interval during the early 1800s reported by Gagan et al. (2000) is well simulated (not shown). Keigwin (1996) observed an increase of about 1°C in the Sargasso Sea from the LIA to the 1900s. The simulations show an increase of about 0.8°C (not shown).

3.3 Ocean salinity

On average, the simulated precipitation is less over large areas of the global ocean during the LIA as compared to the industrial era (not shown). There are, however, a few regions where the precipitation is larger during the LIA, namely in the southern Indian and Pacific Oceans. On the other hand, there is little change in the mean evaporation over the oceans between the LIA and the industrial era (not shown). The resulting salinity differences between the LIA and the industrial era in the upper ocean are small south of 45°N and do not extend to the deeper ocean (Fig. 5a). As mentioned in Sect. 2.1, we note again that climatological winds are used for moisture advection and the calculation of the turbulent fluxes. The hydrological cycle is also simplified in the UVic ESCM. Thus, only small changes in evaporation and percipitation are expected.

In the northern high latitudes (north of 45°N) below 200 m, the salinity on average is lower during the LIA (Fig. 5a). This result is a wind-driven effect since this feature is seen in Fig. 5a and not in Fig. 5b. In the Atlantic basin, the meridional velocity between 200 m and 1,000 m is increased south of 60°N during the industrial era (not shown), resulting in the advection of more salty water from the North Atlantic into the subsurface Arctic.

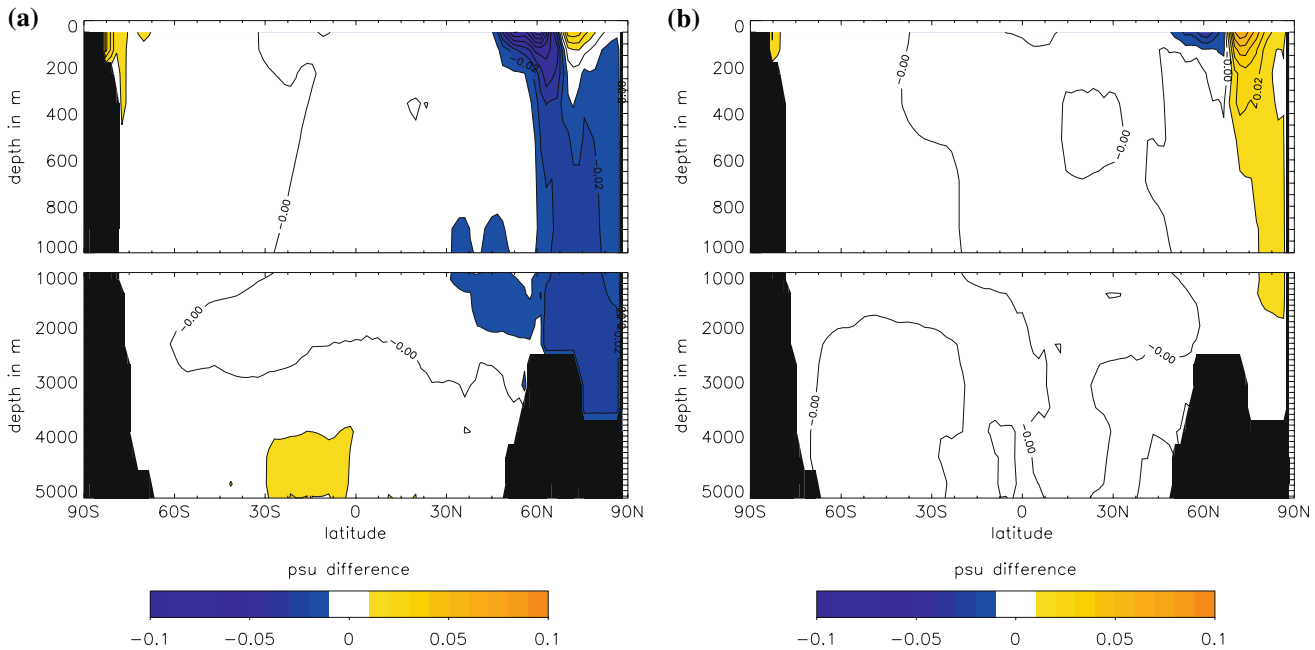

Fig. 5 Latitude-depth structure of the difference of the zonal mean annual global ocean salinity consisting of the mean of 1500 to 1850 minus the mean of 1850 to 2000 for the ANAW wind-stress field. **a** the VOLSOLGHG run; **b** the VOLSOLGHG run minus the CONTR run

We also found that the simulated precipitation over land in the high northern latitudes does not change substantially during the two time periods in the UVic ESCM (not shown). Thus, this suggests that the modelled river runoff into the Arctic Ocean does not result in long-term changes to the salinity.

During the LIA, the water in the Atlantic basin is slightly fresher in a layer at a depth of around 2,000 m extending from 60°N to around 60°S. Because the changes in this layer are very small in the Pacific and Indian basins, this feature can be barely seen in Fig. 5a. This feature can be related to ocean circulation changes which were influenced by changes of the wind-stress at the surface. The higher (global) salinity at the bottom between 30°S and the equator during the LIA (Fig. 5a) originates in the Indian Ocean and is due mainly to wind forcing.

In the upper 200 m north of 50°N, the simulated mean salinity during the two periods shows the signature of a changing sea–ice cover. SM2008 showed that in the Northern Hemisphere, the sea–ice cover is larger during the LIA than in the industrial era. The increased formation of ice in the Arctic basin during the LIA results in a saltier upper Arctic Ocean because of enhanced salt rejection (see Fig. 5b). In addition, southward transport of thicker ice results in a freshening of the upper ocean in the export region during the LIA.

In the upper part of the Ross Sea (south of 75°S), the water is slightly saltier during the LIA (see upper left hand corners of Fig. 5a, b). However, this feature is confined to a small region and does not penetrate beyond a depth of 200 m. The sea–ice cover changes everywhere in the Southern Hemisphere are mainly caused by variable wind forcing, and changes in thermodynamic ice growth and melt play a secondary role (SM2008). Thus, there is no significant change in salinity between the two periods due to sea–ice changes around Antarctica.

Reconstructions from the Indio-Pacific region shows a rapid increase in salinity at the end of the LIA (Newton et al. 2006), while the Tropical Pacific region shows a decrease (Hendy et al. 2002). These changes in salinity are linked to changes in the location of the Inter-Tropical Convergence Zone (e.g., Haug et al. 2001). Since the model has a prescribed wind-stress field, these changes are not simulated.

3.4 Ocean density

The simulated change in ocean density from the LIA to the industrial era is basically a composite of the temperature and the salinity changes shown in Figs. 4 and 5, respectively. In Fig. 6 the potential density is shown relative to σ_1, which is the potential density at the pressure level of 10 MPa (roughly the pressure at a depth of 100 m). The simulated upper ocean potential density during the LIA is greater between 60°S and 50°N down to a depth of 600 m (Fig. 6a), largely because of the colder temperature there (Fig. 4a). This change in density is radiatively driven (Fig. 6b).

In the subsurface Arctic Ocean during the LIA, the density is less on average due to the reduced northward

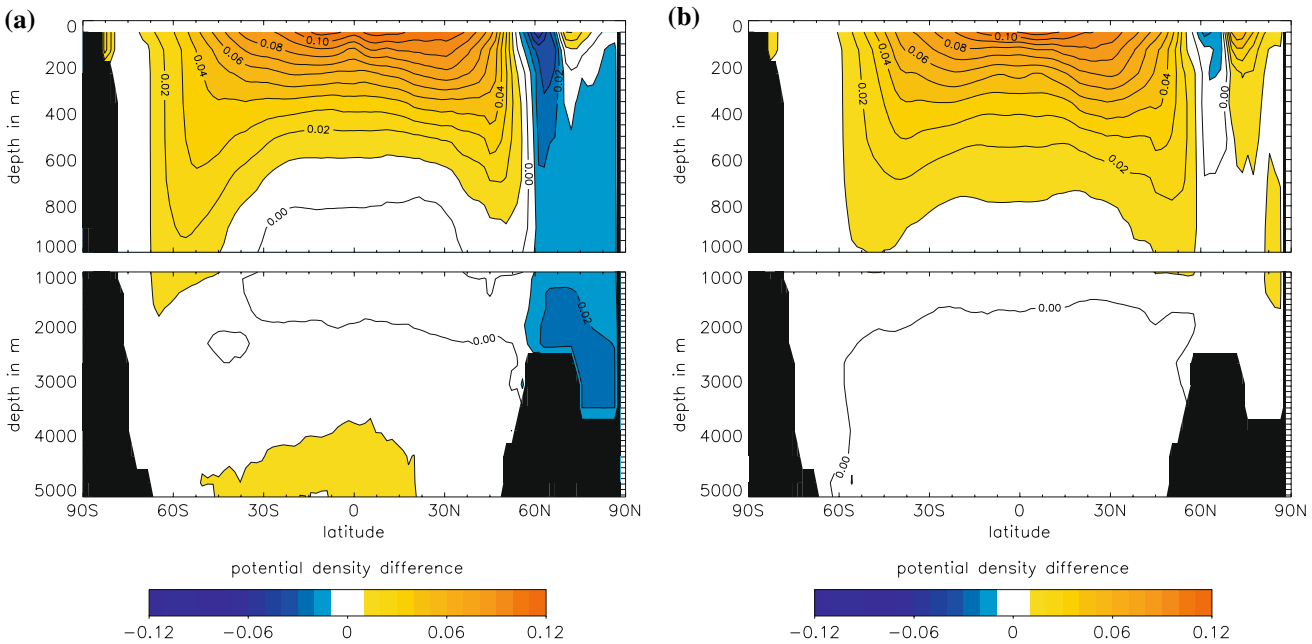

Fig. 6 Latitude-depth structure of the difference of the zonal mean density of the global ocean consisting of the mean of 1500 to 1850 minus the mean of 1850 to 2000. **a**, the VOLSOLGHG run; **b** the VOLSOLGHG run minus the CONTR run

salinity advection during this time period (see Fig. 5a). In the upper Arctic Ocean the larger density during the LIA (Fig. 6a) is connected to the increased salt rejection then. At around 60°N the reduced density during the LIA is produced by more freshwater input from the export of thicker ice.

The denser water during the LIA at the bottom in the tropics and subtropics (Fig. 6a) is mainly produced by colder waters in the Pacific Ocean and saltier waters in the Indian Ocean. Both are wind-driven.

3.5 Meridional overturning circulation

Throughout the simulated period, the Northern Hemisphere maximum AMOC value is located at around 40°N at a depth of 1,800 m (Fig. 7a, b). The difference in AMOC between the industrial era (Fig. 7a) and the LIA (Fig. 7b) indicates that there is a decreased northern sinking branch centered at around 45°N during the LIA (see Fig. 7c). SM2008 showed that the strength of the AMOC is linked to changes in equator to pole temperature gradient. However, the changes

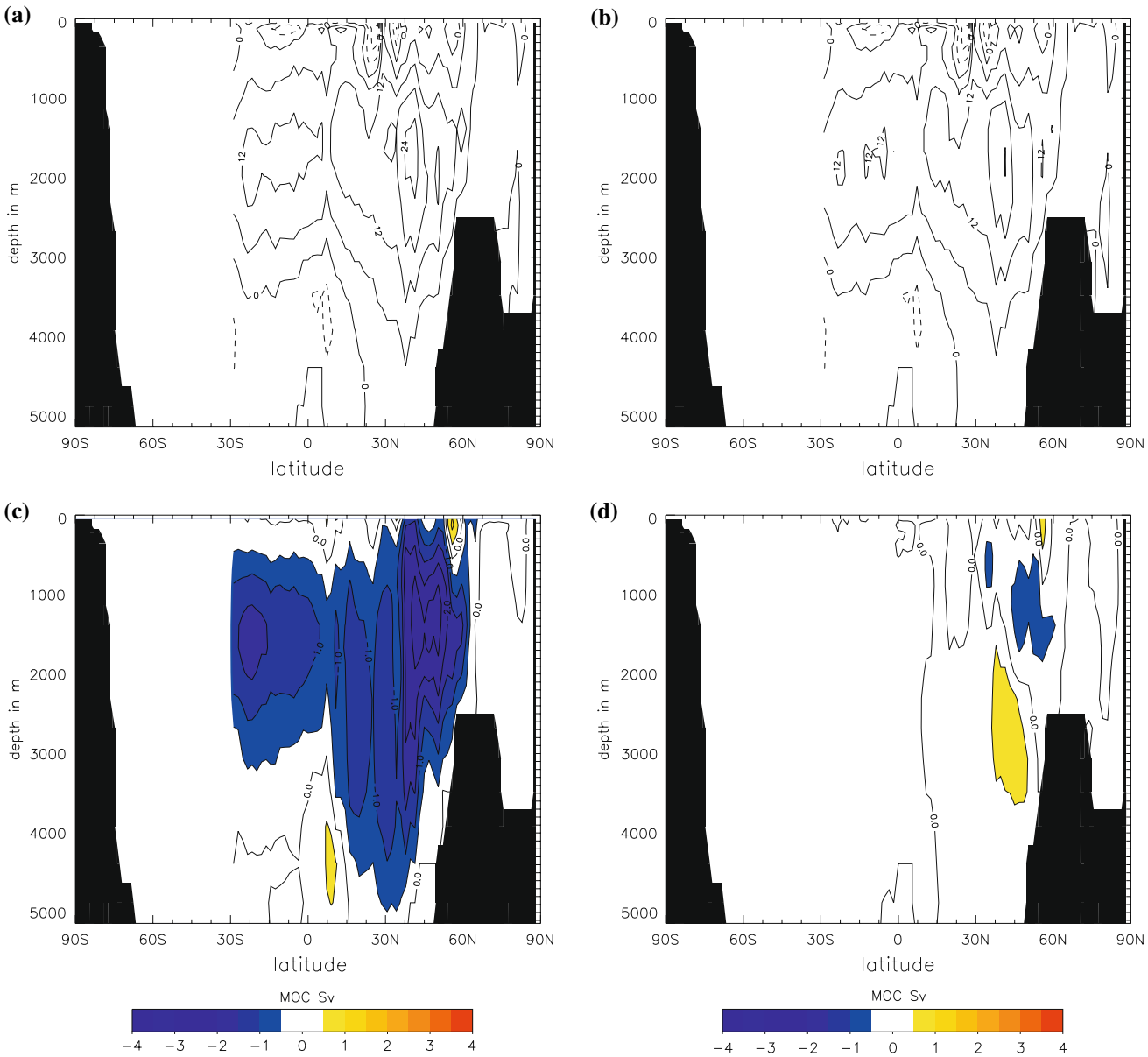

Fig. 7 **a** The mean AMOC for the industrial era; **b** the mean AMOC for the LIA. In both cases the data are from the VOLSOLGHG run with the ANAW wind-stress fields. **c** and **d** AMOC difference of the global ocean consisting of the mean of 1500–1850 minus the mean of 1850–2000 with the ANAW wind-stress field. **c** Output from the VOLSOLGHG run; **d** the difference consisting of the VOLSOLGHG run minus the CONTR run

in prescribed radiative forcing do not significantly change the maximum AMOC in the North Atlantic (Fig. 7d). In the Atlantic basin, the CONTR run maximum AMOC increases by 2.6 Sv from the LIA to the industrial era (not shown). The change of the maximum AMOC in the DECOMP run is smaller, with the increase being 1.3 Sv between these two periods. To determine whether the simulated change in the maximum AMOC is due to the wind forcing or due to the spin-up, we performed an additional ANAW CONTR run which starts from a longer spin-up of 1,500 year. The change in maximum AMOC in this case is 3.0 Sv between the two periods, which is close to the change in the original ANAW CONTR run. These changes in AMOC from one period to the other are between 5 and 10% of the mean maximum AMOC value for each period.

SM2008 showed that the positive sea–ice volume anomaly that occurs in the difference between the CONTR run and the VOLSOLGHG run has little effect on the maximum strength of the AMOC. The simulated increase in the Ekman cell strength around 60°N in the industrial era (Fig. 7c, d) is due to a reduction in sea–ice cover. Over a sea–ice covered area the stress applied on the ocean is modified by the sea ice. Thus, the change in sea–ice cover between the LIA and the industrial era in this region results in a change in wind stress over the ocean.

In the Southern Hemisphere, the Deacon Cell between 52°S and 65°S (the cell in these latitudes with positive contour values in Fig. 8a, b) is enhanced during the LIA, as is the Antarctic Cell south of 65°S (the cell with negative contour values in Fig. 8a–c). Note that in Fig. 8c the changes of the MOC are both negative and positive, however due to a different background state (Fig. 8a, b) the changes in amplitude are of the same sign. The simulations suggest that the Antarctic Cell is 3 Sv stronger during the LIA as compared to the industrial era. In the DECOMP run the change is somewhat smaller, about 1.6 Sv. The ANAW simulation which started from the long spin-up shows a change of 2.6 Sv in the Antarctic Cell.

The wind stress over the Southern Ocean determines the Ekman pumping in the Deacon Cell and hence the divergence of the water mass at the surface. One part of the upper ocean flows into the Antarctic Cell and the other part flows northwards. The mean zonal wind stress in the Southern Ocean is 3.1% stronger in the ANAW simulation during the LIA as compared to the industrial era (not shown). Similarly, for the DECOMP simulation, the wind stress is stronger but only by 0.9%. An additional CONTR run was performed using random winds, as in the spin-up, for the 500-year period. In this run the wind stress over the Southern Ocean is on average 1.2% weaker during the LIA as compared to the industrial era. The resulting change in strength of the Antarctic Cell between the LIA and the industrial era is 0.5 Sv.

The circulation in the Pacific sector is quite strong, as can be deducted from Figs. 7a, b and 8a, b. This property is also visible in the climatological mean MOC of the UVic ESCM (Weaver et al. 2001). The circulation changes in the Pacific sector from the LIA to the industrial era are mostly located south of 45°S.

The MOC changes induced by the radiative forcing show a large negative patch between 60°S and the equator (Fig. 8d). This feature is mainly caused by stronger flow in the Pacific basin during the LIA (not shown).

4 Discussion

4.1 Shortcomings of the simulations

As seen in the previous section, the changes in the ocean properties (between the LIA and the industrial era) due to changes in the radiative forcing are mostly confined to the upper 1,000 m of the ocean. The changes in the deeper ocean are mainly driven by the changes in the winds, i.e., these ocean changes are present in the CONTR run and also are similarly present in the VOLSOLGHG run. Here we would like to discuss two shortcomings of the model simulations which could affect the results for the deeper ocean.

As stated in Sect. 2.1, we have neglected brine convection in our model. Sea–ice in the Arctic Ocean is formed mainly inside the Arctic basin and exported to lower latitudes. Thus, inclusion of brine convection will change the salt content in the Arctic Ocean, but have little impact where sea ice is exported. This finding is supported by Saenko et al. (2002) in a sensitivity study of different brine convection parameterizations using the same model (except for the sea–ice rheology) as in this study. They showed that the NADW is not substantially altered with the inclusion of brine convection. In the Southern Ocean, on the other hand, brine convection is an important factor in forming different water masses. Saenko et al. (2002) showed that the inclusion of a brine convection parameterization improves the representation of Antarctic Intermediate Water and AABW. The surface waters become fresher and the deep waters more saline due to brine convection.

During the 500-year simulation, the mean sea–ice cover in the Southern Ocean is mostly influenced by wind forcing and the changes due to thermodynamic growth or melt play a minor role (SM2008). The sea–ice area is slightly increased during the LIA near the Ross Sea and near the Antarctic Peninsula; however, the simulated sea–ice thickness does not change substantially between the two periods (not shown). The sea–ice area changes can be associated with changes in wind-stress forcing between the

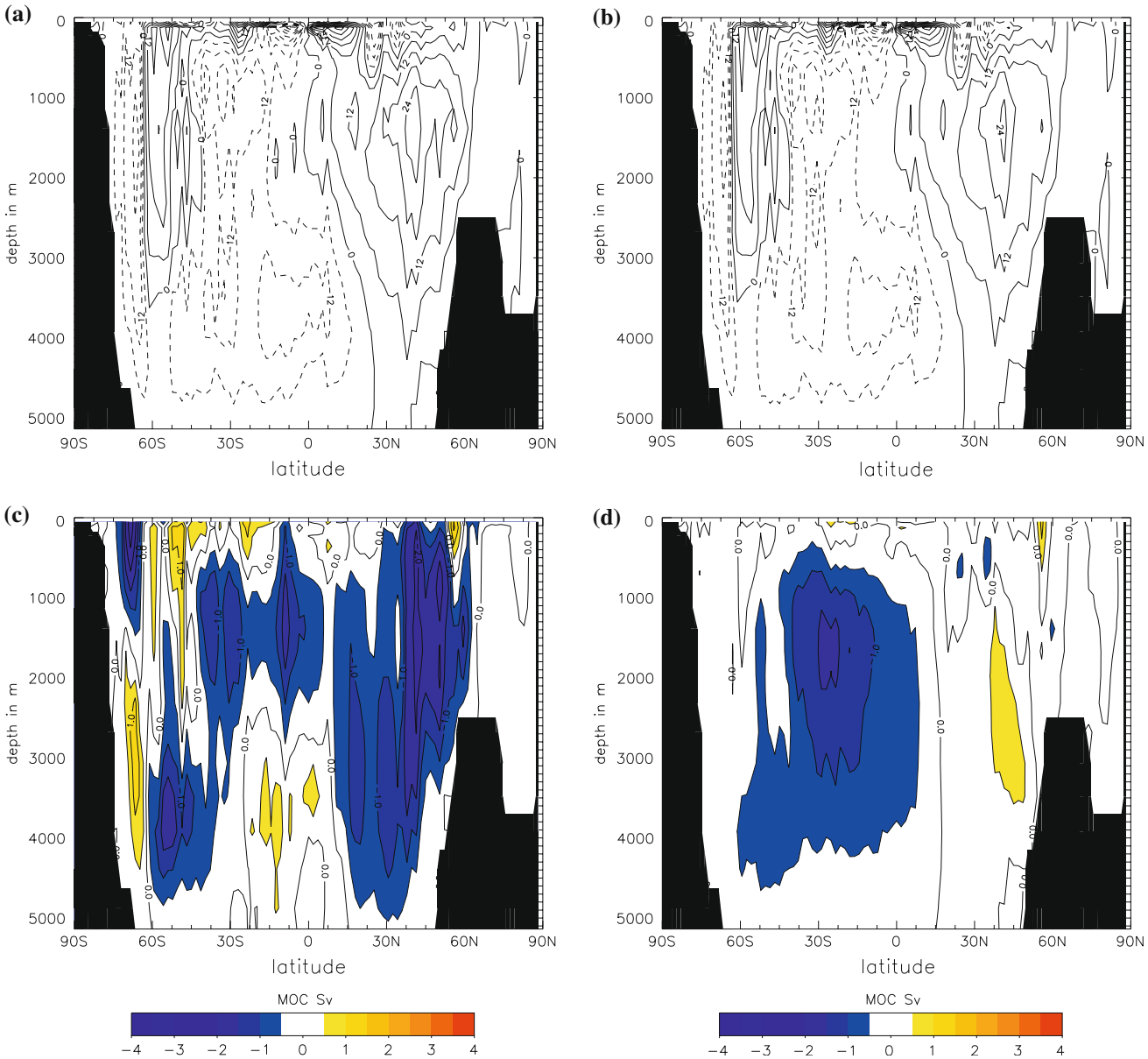

Fig. 8 The same as in Fig. 7 but for the global MOC

two periods. If brine convection were included in the model simulations, more dense water would be produced at the bottom of the Southern Ocean during the LIA.

The second shortcoming in the simulations is the non-interactive wind-stress field. The wind-stress forcings used in this study take into consideration, at least to a certain degree, variations due to the NAO (the ANAW wind-stress field more so than the DECOMP one). However, several features that are special to the atmospheric circulation during the LIA are not captured. In the next subsection we elaborate more on the atmospheric circulation during the LIA and a possible implication of this circulation.

4.2 Broecker et al. (1999) and Broecker (2000) hypothesis

According to the ocean tracer analysis of Broecker et al. (1999) and Broecker (2000), the Southern Ocean ventilation rate during the LIA was larger than today's ventilation rate. On the other hand, the ventilation rate in the North Atlantic should have been only slightly smaller during the LIA as compared to today's NADW formation rate. Our model simulations presented in Sect. 3.5 show that the AMOC in the North Atlantic is indeed slightly smaller during the LIA and that the Southern Ocean ventilation rate is increased during the LIA as compared to the industrial

period. However, our results suggest that the differences in ventilation rate are associated with changes in atmospheric circulation rather than oceanic changes due to changes in radiative forcing.

In our simulations the mean strength of the Antarctic Cell shows a linear relationship with the mean change in zonal wind stress over the Southern Ocean. However, in order to have such an increased ventilation rate during the LIA as hypothesized by Broecker et al. (1999) and Broecker (2000), the winds over the Southern Ocean would have had to be even larger than in our simulations.

Thus the question arising is, were the westerlies (i.e., the zonal wind stress) in the Southern Hemisphere stronger during the LIA or were they displaced to a more northward or southward position? More than two decades ago Lamb (1985) suggested that the global atmospheric flow was more zonal during the LIA. (We thus infer this was also true for the Southern Hemisphere.) Furthermore, on the Quelccaya ice cap in Peru, Thompson et al. (1986) observed stronger westerly or northwesterly winds during the LIA. Susceptibility measurements near the Antarctic Peninsula, on the other hand, suggest that there were either stronger surface westerly winds or a southward displacement of the surface westerlies during that period (Shevenell and Kennett 2002). This is in line with observations from Hendy et al. (2002), which indicate that the meridional temperature gradient was increased during the LIA and hence the thermal wind was enhanced. However, from the analysis of ice cores, Kreutz et al. (1997) suggested that there could have been an expanded southern polar vortex or an increased meridional circulation after 1400 which lasted well into the twentieth century.

During strong westerly events in the Southern Hemisphere, the Antarctic Peninsula is warmer than average and mainland Antarctica is colder than average (Rogers 1983). Indeed, after 1500 such a dipole pattern in temperature proxies was observed over the Antarctic continent (Mosley-Thompson 1995). During most of the LIA the Antarctic Peninsula was warmer and the mainland temperatures were decreased. After the nineteenth century the long-term temperature trends changed sign.

From the proxy evidence mentioned above it is unclear if there was a strengthening or a southward displacement of the surface westerlies in the Southern Hemisphere. As seen in Sect. 3.5, a stronger zonal wind stress results in an increased ventilation rate in the Antarctic Cell. Also, stronger winds result in increased generation of transient eddies which could renew more often the sea–ice cover and hence increase the amount of brine rejected. On the other hand, a southward displacement of the westerlies could shift the location of the maximal zonal wind stress closer to the Antarctic Circumpolar Current region. The resulting effect would be similar as strengthening the westerlies.

Both scenarios would increase the Southern Ocean ventilation rate during the LIA as proposed by Broecker et al. (1999) and Broecker (2000). However, to verify which mechanism was in place during the LIA, the use of a more comprehensive atmospheric GCM coupled to an ocean GCM would be needed.

5 Summary

Two different wind-stress fields, which take into account variations of the NAO, and three different radiative forcings (i.e., volcanic activity, greenhouse gas changes and insolation changes) have been used in a global reduced complexity model to investigate the ocean properties such as ocean heat content, temperature, salinity, density and circulation during the LIA and the subsequent industrial era. Furthermore, we assessed the validity of the Broecker et al. (1999) and Broecker (2000) hypothesis of an increased Southern Ocean ventilation rate during the LIA.

According to our simulations, dynamically induced changes to the total ocean heat content essentially eliminate a radiatively forced downward trend in this quantity in the full ocean at the beginning of the LIA (up to 1700). In the upper ocean and after 1700 in the full ocean, the dynamical forcing does not appear to have had a large influence on the global heat content changes. The changes in ocean heat content in both polar regions are likely due to advective events rather than radiatively induced changes. The impact of the cooler LIA on the interior ocean temperature is mostly confined to the upper 1,000 m of the ocean. Changes in the deep ocean temperature are mainly wind-driven.

The salinity changes over the simulated period at the surface due to changes in precipitation and evaporation are small and do not influence the salinity budget in the ocean's interior. During the industrial era, the salinity content increases in the subsurface Arctic Ocean, mainly due to an increased salt advection from the Atlantic basin. In the upper Arctic Ocean, the increased salinity during the LIA reflected the changes in sea–ice cover, i.e., increased sea–ice thickness during the LIA resulted in increased salt rejection. In the North Atlantic region a freshening in the upper ocean occurs during the LIA due to the export and melting of thicker sea ice.

The changes in the latitude-depth structure of the potential density are a composite picture of the salinity and temperature changes in the ocean. During the LIA the water in the subsurface Arctic Ocean is lighter due to the reduced transport of inflowing saline water from the North Atlantic. In the upper Arctic Ocean the water is heavier during the LIA due to increased salt rejection, and in the upper northern North Atlantic the water is lighter during

this time due to export and melt of thicker ice. In the ice-free regions, the ocean is denser in the upper 600 m due to lower temperatures during the LIA.

The simulations show that the maximum AMOC is decreased during the LIA as compared to the industrial era. However, this decrease is mostly wind-driven and the changes due to the radiative forcing are negligible. In the Southern Ocean, the ventilation rate is larger during the LIA as compared to the industrial era, mainly due to an increased average zonal wind stress over that region. In our simulations the increase in zonal wind stress and the ventilation rate in the Antarctic Cell show a linear relationship.

Thompson et al. (1986) and Shevenell and Kennett (2002) observed increased westerly winds or a more southward displacement of the westerlies during the LIA. The increased westerlies would have enhanced the ventilation rate in the Southern Ocean. Additionally, the stronger westerlies which are less stable would increase the frequency of the transient eddies and renew the sea–ice cover more often. Further, more brine would have been rejected and this would have increased even more the ventilation rate of the Southern Ocean. This could be an alternative explanation for the stronger ventilation rate discussed by Broecker et al. (1999) and Broecker (2000). However, simulations with an atmospheric GCM coupled to an ocean GCM would be needed to rigorously verify this proposed mechanism.

Acknowledgments We thank the two anonymous reviewers for their comments and suggestions which helped to improve the paper. This work was supported by an NSERC Discovery Grant awarded to L. A. M. and the NSERC/CFCAS-funded Canadian CLIVAR Research Network.

References

Bitz CM, Holland MM, Weaver AJ, Eby M (2001) Simulating the ice-thickness distribution in a coupled climate model. J Geophys Res 106(C2):2441–2463

Bradley RS, Jones PD (eds) (1995) Climate Since A.D. 1500. Routledge

Broecker WS (2000) Was a change in thermohaline circulation responsible for the Little Ice Age? Proc Natl Acad Sci 97(4):1339–1342

Broecker WS, Sutherland S, Peng TH (1999) A possible 20th-century slowdown of Southern Ocean Deep Water formation. Science 286:1132–1135

Bryan K, Lewis LJ (1979) A water mass model of the world ocean circulation. J Geophys Res 84:2503–2517

Crowley TJ (2000) Causes of climate change over the past 1000 years. Science 289:270–277

Crowley TJ, Baum SK, Kim KY, Hegerl GC, Hyde WT (2003) Modeling ocean heat content changes during the last millennium. Geophys Res Lett 30(18). doi:10.1029/2003GL017801

Delworth TL, Greatbatch RJ (2000) Multidecadal thermohaline circulation variability driven by atmospheric surface flux forcing. J Clim 13:1481–1495

Delworth TL, Mann ME (2000) Observed and simulated multidecadal variability in the Northern Hemisphere. Clim Dyn 16:661–676

Delworth T, Manabe S, Stouffer R (1993) Interdecadal variations of the thermohaline circulation in a coupled ocean-atmosphere model. J Clim 6:1993–2011

Fanning AF, Weaver AJ (1996) An atmospheric energy-moisture balance model: climatology, interpentadal climate change, and coupling to an ocean general circulation model. J Geophys Res 101(D10):15,111–15,128

Gagan MK, Ayliffe LK, Beck JW, Cole JE, Druffel ERM, Dunbar RB, Schrag DP (2000) New views of tropical paleoclimates from corals. Quat Sci Rev 19:45–64

Gill AE (1982) Atmosphere–ocean dynamics. Academic Press, London

Grove JM (2004) Little ice ages: ancient and modern, Routledge studies in physical geography and environment, vol 5, 2nd edn. Routledge

Haug GH, Hughen KA, Sigman DM, Peterson LC, Röhl U (2001) Southward migration of the Intertropical Convergence Zone through the Holocene. Science 293:1304–1308

Hendy EJ, Gagan MK, Alibert CA, McCulloch MT, Lough JM, Isdale PJ (2002) Abrupt decrease in tropical Pacific sea surface salinity at end of Little Ice Age. Science 295:1511–1514

Holland MM, Bitz CM, Eby M, Weaver AJ (2001) The role of ice-ocean interactions in the variability of the North Atlantic thermohaline circulation. J Clim 14:656–675

Jones PD, Mann ME (2004) Climate over the past millennia. Rev Geophys 42. doi:10.1029/2003RG000143

Keigwin LD (1996) The Little Ice Age and Medieval warm period in the Sargasso Sea. Science 274(5292):1504–1508

Keigwin LD, Boyle EA (2000) Detecting Holocene changes in thermohaline circulation. Proc Natl Acad Sci 97(4):1343–1346

Kreutz KJ, Mayewski PA, Meeker LD, Twickler MS, Whitlow SI, Pittalwala II (1997) Bipolar changes in atmospheric circulation during the Little Ice Age. Science 277:1294–1296

Kushnir Y (1994) Interdecadal variations in North Atlantic sea surface temperature and associated atmospheric conditions. J Clim 7:141–157

Lamb HH (1985) Climatic history and the future. Princeton University Press, Princeton

Levitus S, Antonov J, Boyer T (2005) Warming of the world ocean, 1955–2003. Geophys Res Lett 32. doi:10.1029/2004GL021592

Lund DC, Lynch-Stieglitz J, Curry WB (2006) Gulf Stream density structure and transport during the past millennium. Nature 444:601–604, doi:10.1038/nature05277

Luterbacher J, Xoplaki E, Dietrich D, Jones PD, Davies TD, Portis D, González-Rouco JF, von Storch H, Gyalistras D, Casty C, Wanner H (2002a) Extending North Atlantic Oscillation reconstructions back to 1500. Atmos Sci Lett 2:114–124. doi:10.1006/asle.2001.0044

Luterbacher J, Xoplaki E, Dietrich D, Rickli R, Jacobeit J, Beck C, Gyalistras D, Schmutz C, Wanner H (2002b) Reconstruction of sea level pressure fields over the Eastern North Atlantic and Europe back to 1500. Clim Dyn 18:545–561. doi:10.1007/s00382-001-0196-6

Marotzke J, Welander P, Willebrand J (1988) Instability and multiple steady states in a meridional-plane model of the thermohaline circulation. Tellus 40A(2):162–172

Mosley-Thompson E (1995) Paleoenvironmental conditions in Antarctica since A.D. 1500: ice core evidence. In: Bradley RS, Jones PD (eds) Climate Since A.D. 1500, Routledge, Chap 29

Mysak LA, Wright KM, Sedláček J, Eby M (2005) Simulation of sea ice and ocean variability in the Arctic during 1955–2002 with an intermediate complexity model. Atmosphere–Ocean 43(1):101–118

Newton A, Thunell R, Stott L (2006) Climate and hydrograohic variability in the indio-pacific warm pool during the last millennium. Geophys Res Lett 33. doi:10.1029/2006GL027234

Pacanowski R (1995) MOM 2 Documentation User's Guide and Reference Manual, GFDL Ocean Group. Technical Report 3, NOAA, GFDL

Pfister C (1995) Monthly temperature and precipitation in central Europe 1525–1979: quantifying documentary evidence on weather and its effects. In: Bradley RS, Jones PD (eds) Climate Since A.D. 1500, Routledge, Chap 6

Rahmstorf S, England MH (1997) Influence of Southern Hemisphere winds on North Atlantic deep water flow. J Phys Oceanogr 27:2040–2054

Rogers JC (1983) Spatial variability of Antarctic temperature anomalies and their association with Southern Hemisphere atmospheric circulation. Ann Assoc Am Geogr 73(4):502–518

Saenko OA, Flato GM, Weaver AJ (2002) Improved representation of sea–ice processes in climate models. Atmosphere–Ocean 40(1):21–43

Schlesinger ME, Ramankutty N (1994) An oscillation in the global climate system of period 65–70 years. Nature 367:723–726. doi:10.1038/367723a0

Sedláček J, Mysak LA (2008) Sensitivity of sea ice to wind-stress and radiative forcing since 1500: a model study of the Little Ice Age and beyond. Clim Dyn. doi:10.1007/s00382-008-0406-6

Sedláček J, Lemieux JF, Mysak LA, Tremblay LB, Holland DM (2007) The granular sea–ice model in spherical coordinates and its application to a global climate model. J Clim 20(24):5946–5961. doi:10.1175/2007JCLI1664.1

Shevenell AE, Kennett JP (2002) Antarctic Holocene climate change: a benthic foraminiferal stable isotope record from Palmer Deep. Paleoceanography 17(2), doi:10.1029/2000PA000596

Stommel H (1961) Thermohaline convection with two stable regimes of flow. Tellus 8(2):225–230

te Raa LA, Dijkstra HA (2002) Instability of the thermohaline ocean circulation on interdecadal timescales. J Phys Oceanogr 32:138–160

te Raa L, Gerrits J, Dijkstra HA (2004) Identification of the mechanism of interdecadal variability in the North Atlantic ocean. J Phys Oceanogr 34:2792–2807, doi:10.1175/JPO2655.1

Thompson LG, Mosley-Thompson E, Dansgaard W, Grootes PM (1986) The Little Ice Age as recorded in the stratigraphy of the tropical Quelccaya ice cap. Science 234(4774):361–364

Timmermann A, Goosse H (2004) Is the wind stress forcing essential for the meriodional overturning circulation? Geophys Res Lett 31. doi:10.1029/2003GL018777

Toggweiler JR, Samuels B (1995) Effect of Drake Passage on the global thermohaline circulation. Deep-Sea Res I 42(4):477–500

Tremblay LB, Mysak LA (1997) Modeling sea ice as a granular material, including the dilatancy effect. J Phys Oceanogr 27:2342–2360

Weaver AJ, Eby M, Wiebe EC, Bitz CM, Duffy PB, Ewen TL, Fanning AF, Holland MM, MacFadyen A, Matthews HD, Meissner KJ, Saenko O, Schmittner A, Wang H, Yoshimori M (2001) The UVic earth system climate model: model description, climatology, and applications to past, present and future climates. Atmosphere–Ocean 39(4):361–428

Zorita E, von Storch H, González-Rouco FJ, Cubasch U, Luterbacher J, Legutke S, Fischer-Bruns I, Schlese U (2004) Climate evolution in the last five centuries simulated by an atmosphere–ocean model: global temperatures, the North Atlantic Oscillation and the Late Maunder Minimum. Metereologische Zeitschrift 13(4):271–289